Structural development during deformation of polyurethane containing polyhedral oligomeric silsesquioxanes (POSS) molecules

B.X. Fu[a], B.S. Hsiao[a],*, S. Pagola[b], P. Stephens[b], H. White[c], M. Rafailovich[c], J. Sokolov[c], P.T. Mather[d], H.G. Jeon[e], S. Phillips[f], J. Lichtenhan[g], J. Schwab[g]

[a]*Department of Chemistry, State University of New York at Stony Brook, Stony Brook, NY 11794-3400, USA*
[b]*Department of Physics, State University of New York at Stony Brook, Stony Brook, NY 11794-3400, USA*
[c]*Department of Materials Science and Engineering, State University of New York at Stony Brook, Stony Brook, NY 11794-3400, USA*
[d]*Materials and Manufacturing Directorate, Air Force Research Laboratory, Wright Patterson AFB, OH 45433-7750, USA*
[e]*Systran Corporation, Air Force Research Laboratory, Wright Patterson AFB, OH 45433-7750, USA*
[f]*Propulsion Directorate, Air Force Research Laboratory, Edwards AFB, CA 93524-7680, USA*
[g]*Hybrid Plastics, 18237 Mt. Baldy Circle, Fountain Valley, CA 92708-6117, USA*

Abstract

A unique polyurethane (PU) elastomer containing inorganic polyhedral oligomeric silsesquioxane (POSS) molecules as molecular reinforcements in the hard segment was investigated by means of wide-angle X-ray diffraction (WAXD), small-angle X-ray scattering (SAXS) and transmission electron microscopy (TEM) techniques. The mechanical properties of POSS modified polyurethane (POSS-PU) were also compared to those of polyurethane without POSS. The crystal structures of two different POSS molecules were first determined by X-ray powder diffraction analysis, yielding a rhombohedral cell with $a = 11.57$ Å, $\alpha = 95.5°$ for octacyclohexyl-POSS (1,3,5,7,9,11,13,15-octacyclohexylpentacyclo[9.5.1.13,9.15,15.17,13] octasiloxane) and $a = 11.53$ Å, $\alpha = 95.3°$ for hydrido-POSS (1-[hydridodimethylsiloxy]-3,5,7,9,11,13,15-heptacyclohexylpentacyclo [9.5.1.13,9.15,15.17,13] octasiloxane). WAXD results showed that reflection peaks distinct to POSS crystal diffraction were seen in POSS-modified polyurethane, which suggests that POSS molecules formed nanoscale crystals in the hard domain. During deformation, the average size of POSS crystals in POSS-PU was found to decrease while elongation-induced crystallization of the soft segments was observed at strains greater than 100%. The SAXS results showed microphase structure typical of segmented polyurethanes, with an initial long spacing of 110 Å between the domains. At high strains, the average length of strain-induced microfibrillar soft-segment crystals was estimated to be about 60 Å by SAXS. The TEM analysis of highly stretched samples showed a preferred orientation of deformed hard domains perpendicular to the stretching direction, indicating the destruction of hard segment domains by strain. © 2000 Published by Elsevier Science Ltd.

Keywords: Polyhedral oligomeric silsesquioxane; Polyurethane; Nanocomposites

1. Introduction

Segmented polyurethane-based elastomers have excellent mechanical and thermophysical properties, such as high tensile strength, large reversible elongation, and enhanced rubbery modulus. It is now widely accepted that the superior properties in these copolymers are directly related to the formation of microphase separation from the thermo-dynamic incompatibility (immiscibility) of solid-like hard segments and rubbery soft segments [1–3]. The hard segments usually involve interchain interactions by means of van der Waals forces and hydrogen bonding, which determine the macroscopic properties. It is the intermolecular association of the hard segments that provides the physical crosslinking to the system.

Considerable academic and industrial efforts have been focused on studying the structure-property relationships in segmented polyurethanes. A commercially important class of polyurethanes containing crystallizable 4,4′-methylene-bis (phenylisocyanate) (MDI) hard segments, polytetramethylene glycol (PTMG) soft segments and a chain extender of 1,4-butanediol (BD) has been studied most extensively. Several studies have successfully developed similar structural models for the microphase separation of hard and soft segments in this polymer system, based
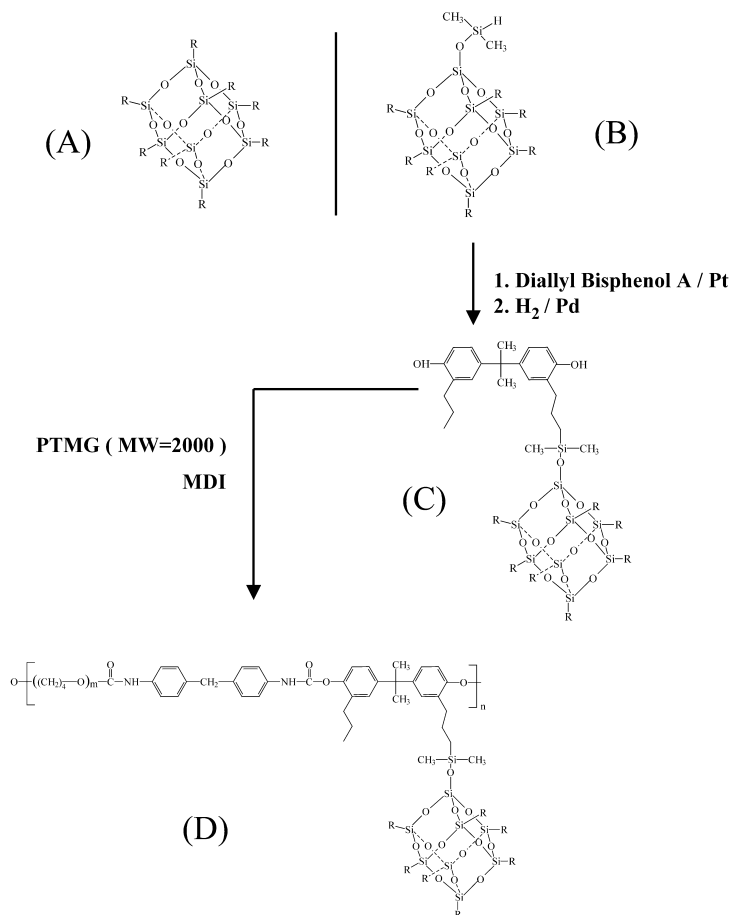

Fig. 1. Schematic diagram of the synthesis for POSS-polyurethane: (A) octacyclohexyl-POSS, with R = cyclohexyl; (B) hydrido-POSS; (C) BPA-POSS; and (D) POSS-PU.

primarily on results from wide-angle X-ray diffraction (WAXD) and small-angle X-ray scattering (SAXS) [4–8].

In this study, a polyurethane system containing polyhedral oligomeric silsesquioxane (POSS) cage-like molecules pendent to the polymer chain has been investigated. The copolymer consists of random sequences of PTMG soft segments and 4,4′-methylenebis (phenylisocyanate) (MDI) hard segments. The MDI hard segment was chain-extended by 1-[3-(propylbisphenolA)propyldimethylsiloxy]-3,5,7,9, 11,13,15 heptacyclohexylpentacyclo-[9.5.1.13,9.15,15.17,13] octasiloxane (BPA-POSS) (Fig. 1). The unique properties of this polymer are brought about by the POSS molecules reinforcing the hard segment domains at the molecular level. Previous studies have shown that such organic-inorganic hybrid polymers possess improved properties such as higher T_g, increased oxygen permeability, reduced flammability and enhanced mechanical strength [9–14].

The POSS molecule contains a polyhedral silicon–oxygen nanostructured skeleton with intermittent siloxane chains (general formula $(SiO_{3/2})_n$) [15–20], which was first reported in 1946 [21]. Silsesquioxanes have the empirical formula $RSiO_{1.5}$, with their name being derived from the non-integer (one and one-half or *sesqui*) ratio between oxygen and silicon atoms, and the organic substituent. A variety of substituents can be incorporated on the silicon atom, with recent interest focusing on the incorporation of a polymerizable group on one of the silicon atoms, and aliphatic hydrocarbon group on the remaining silicon atoms, to impart desirable solubility properties. These molecules have come to be known as polyhedral oligomeric silsesquioxanes, or POSS monomers and can be polymerized to the corresponding POSS macromers and polymers.

The POSS molecules have been successfully incorporated into different polymers such as styryls, acrylics, liquid crystalline polyesters, siloxanes and polyamides, etc. by scientists from the Air Force Research Laboratory (AFRL) [9–15]. In this study, the chosen POSS molecule $(SiO_{3/2})_n$ has $n = 8$ (cage-like), with the corner group as cyclohexyl (molecular weight greater than 1000 amu). This molecule is considered large (approximately 15 Å in molecular axis, with an inner Si–Si diameter of 5.4 Å) as compared to the regular size of polyurethane hard domains (25 Å) [22]. Our goal in this study is to understand the effect of POSS molecules on both microscopic and macroscopic properties.
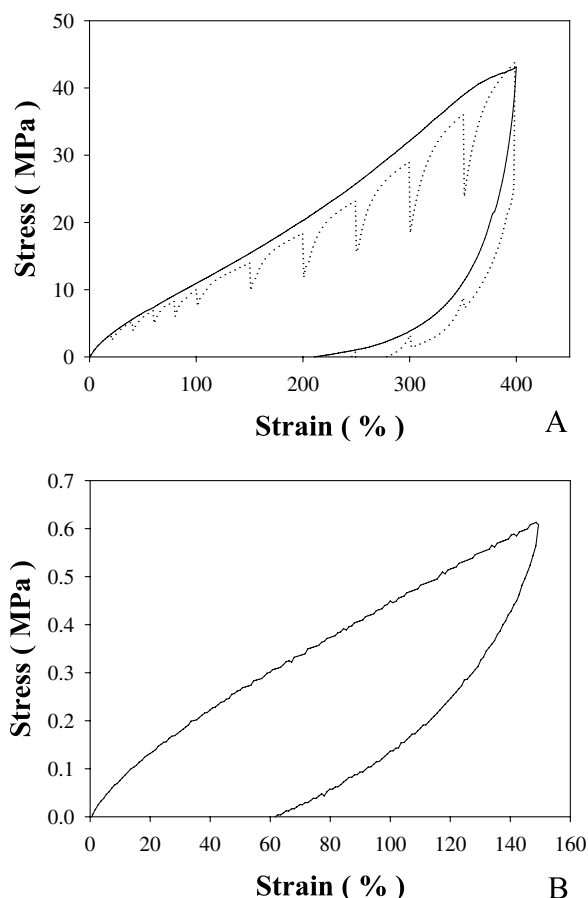
Fig. 2. Stress-strain curves for cyclic deformation of: (A) POSS-PU-34; and (B) POSS-PU-0. (The dotted line in (A) represents the stretch-hold condition for X-ray measurement. The sample was allowed to relax for 10 min at varying strains.)

2. Experimental

The chosen basic POSS molecular structure $(SiO_{3/2}R)_8$ contains R = cyclohexyl (octacyclohexyl-POSS). We have also investigated its derivative with one corner group substituted by: (1) hydridomethylsiloxy group (hydrido-POSS) and (2) 3-(allylbisphenol-A) propyldimethylsiloxy group (BPA-POSS). The BPA-POSS compound is a diol, which was used in the polyurethane synthesis as a chain extender. The POSS-polyurethane (POSS-PU) contains soft segments of PTMG ($M_w = 2000$), and hard segments of 4,4′-methylenebis (phenylisocyanate) (MDI) and BPA-POSS. As prepared, the sample contains 34 weight percent POSS molecules (POSS-PU-34). A reference sample with no POSS (POSS-PU-0) was also synthesized for comparison. The synthesis method was published in a previous paper [22]. The synthesis followed a typical synthetic scheme is shown in Fig. 1.

An Instron 4400 tensile apparatus was used to determine the mechanical properties of POSS-PU and to collect the in situ X-ray images during deformation. The stretching speed used was 5 mm/min. For the deformation study, the POSS-PU film and the reference polyurethane film having the width, thickness and length of 3, 1, 10 mm, respectively, were prepared by compression molding ($\sim$200°C). Samples were held still and relaxed for 10 min as they reached the desired stretching ratio for X-ray measurements. All deformation experiments were carried out at room temperature.

Simultaneous WAXD and SAXS measurements during deformation were carried out at the Advanced Polymers beamline, X27C, National Synchrotron Light Source (NSLS), Brookhaven National Laboratory (BNL). A double multilayer monochromator was used to generate monochromatic X-rays with a wavelength of 1.307 Å. The beam size was about 0.6 mm in diameter at the sample position, which was defined by a pinhole collimator. Two Fuji imaging plates were used to detect both WAXD (having a central opening allowing the passage of the SAXS signals) and SAXS images simultaneously. The chosen sample-to-detector distance for WAXD was 140 mm and for SAXS was 1190 mm. The WAXD profiles were calibrated by a silicon standard, while SAXS profiles were calibrated by silver behenate.

For the crystal structure analysis, wide-angle X-ray powder diffraction experiments were also carried out using a four-circle diffactometer in the SUNY beamline, X3B1, in NSLS, BNL. The wavelength used was 1.151 Å (via a double crystal monochromator). The maximum attainable diffraction angular range was 60 degrees. The structural refinement was carried out using a custom code for the analysis of powder diffraction data.

Morphological observation was done by transmission electron microscopy (TEM). Both unstretched and stretched POSS-PU-34 films were sectioned ($\sim$700 Å thickness) at -50°C, using a cryo-microtome, with a diamond knife. For stretched films, the following procedure for sample preparation was used. Compression molded films were cut into strips in 1 mm thick, 3 mm wide and 10 mm long. The films were then mounted in a custom drawing apparatus. The mounted films were then stretched to a tensile strain of 700% at a constant draw rate ($\sim$5 cm/s) and at room temperature, followed by annealing under tension for five days at room temperature. After unloading the stretched films, relaxation occurred to give a tensile strain of $\sim$500% based on the original length. The stretched and relaxed films thus prepared were used for cryo-microtoming. Bright field images of microdomain structures were observed with a Philips CM200 operated at 200 kV. These samples are unstained and that the contrast is from scattering (as opposed to phase contrast).

3. Results and discussion

3.1. Mechanical behavior

The tensile properties of segmented polyurethane depend upon the chemical structure, the copolymer composition,
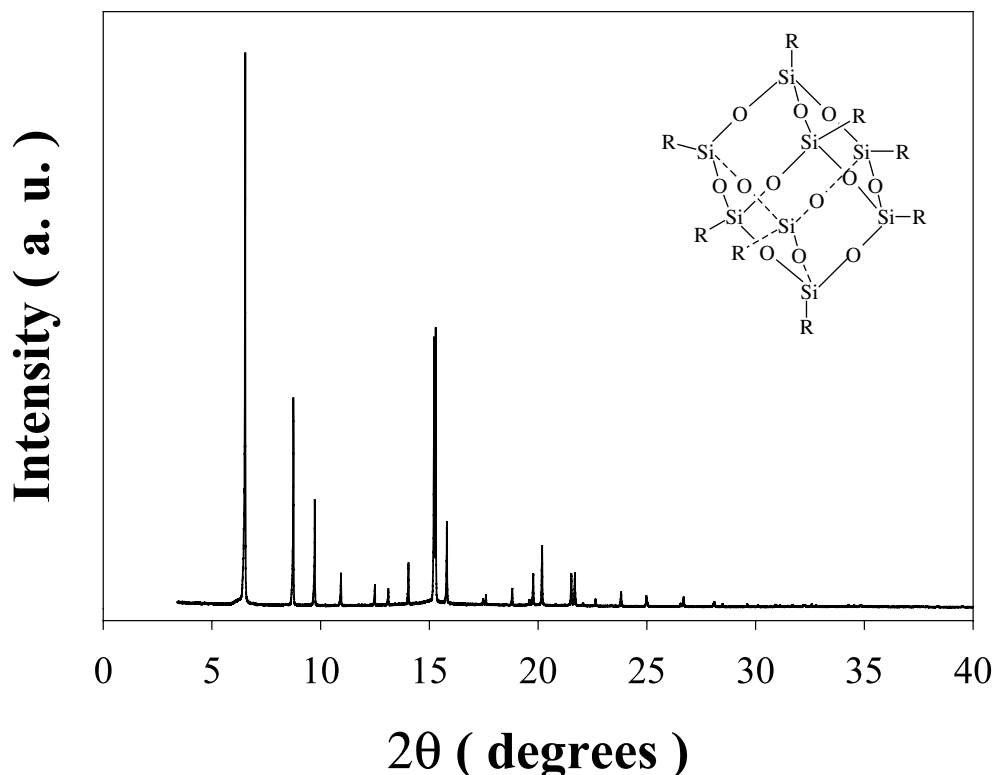
Fig. 3. The X-ray powder diffraction profile of octacyclohexyl-POSS. The crystal can be indexed by rhombohedral unit cell with $a = 11.57$ Å, $\alpha = 95.5°$.

and the microphase morphology. Typical stress–strain curve of the compression-molded POSS-PU-34 sample obtained from the Instron tensile machine is shown in Fig. 2A (solid line). The reference polyurethane sample without

Table 1
Observed and calculated d-spacings using a rhombohedral cell with $a = 11.57$ Å, $\alpha = 95.5°$ and the measured diffraction intensity from the X-ray powder diffraction pattern obtained from octacyclohexyl-POSS crystals

hkl	d_{obs} (Å)	d_{cal} (Å)	I_0[a]
101	11.49	11.449	VS
110	8.59	8.560	S
012	7.72	7.700	M
021	6.88	6.856	W
003	6.03	6.007	VW
202	5.74	5.725	VW
211	5.37	5.351	W
030	4.96	4.944	VS
113	4.93	4.917	VS
122	4.77	4.759	M
104	4.32	4.310	VW
220	4.29	4.280	VW
131	4.02	4.009	VW
303	3.83	3.816	W
312	3.75	3.741	M
124	3.52	3.511	W
105	3.50	3.502	W
321	3.35	3.342	VW
232	3.19	3.182	VW

[a] VS, very strong; S, strong; M, middle; W, weak; and VW, very weak.

POSS is shown in Fig. 2B for comparison. The maximum applied strain of POSS-PU-34 was about 400% (the maximum attainable strain was about 700%), and the maximum attainable strain of the reference polyurethane sample (POSS-PU-0) was only about 150%. Based on the interpretation of the stress-strain behavior in typical segmented polyurethane provided by Cella [23] and Witsiepe [24], the observed mechanical behavior of POSS-PU-34 may be explained by the following hypothesis. The initial extension may be attributed to the reversible deformation of the crystalline (hard) domains (probably 0–50% in POSS-PU-34). At strains of 50–150% in POSS-PU-34, a partly reversible reorientation of hard domains probably occurs. At higher strains, the stress is transmitted primarily through the amorphous soft segment phase. We intend to test this hypothesis as if it is applicable to the POSS-PU system.

In Fig. 2, by comparing the properties at strains <150%, we find that a significant mechanical improvement is achieved by incorporating the POSS molecules in PU. We also observe that the maximum attainable strain of the reference polyurethane sample is significantly less than that of POSS-PU-34. We attribute the inferior properties in pure PU in part to the thermal degradation of PU after compression molding (~200°C), and in part to the lower molecular weight of the sample resulted from the chosen synthesis [22]. The higher attainable strain in POSS-PU-34 suggests that the POSS inclusion in the chains has enhanced the thermal stability of the PU system and its molecular weight may also be higher. Fig. 2A also illustrates the stress-strain
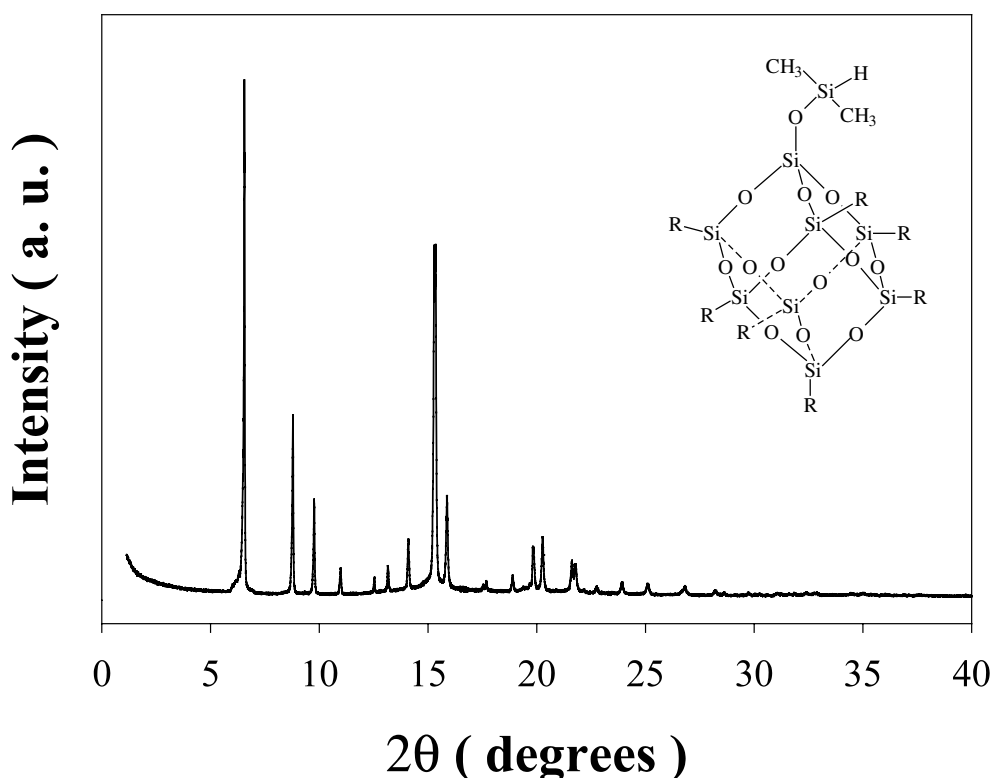
Fig. 4. The X-ray powder diffraction profile of hydrido-POSS. The crystal can be indexed by rhombohedral unit cell with $a = 11.53$ Å, $\alpha = 95.3°$.

relationship obtained when POSS-PU-34 was subjected to a relaxation of 10 min after a programmed strain for WAXD/SAXS measurements was reached. This data, shown as the dashed line, reveals significant strain-rate dependence of the mechanical response. The observed hysterisis behavior

Table 2
Observed and calculated d-spacings using a rhombohedral cell with $a = 11.53$ Å, $\alpha = 95.3°$ and the measured diffraction intensity from the X-ray powder diffraction pattern obtained from hydrido-POSS crystals

hkl	d_{obs} (Å)	d_{cal} (Å)	I_0 [a]
101	11.45	11.421	VS
110	8.55	8.528	S
012	7.70	7.688	M
021	6.85	6.833	W
003	6.00	6.003	VW
202	5.73	5.710	VW
211	5.35	5.333	W
030	4.92	4.924	VS
113	4.92	4.909	VS
122	4.76	4.754	M
104	4.31	4.306	VW
220	4.27	4.264	VW
131	4.00	3.995	VW
303	3.82	3.807	W
312	3.74	3.729	M
124	3.51	3.505	W
105	3.48	3.499	W
321	3.33	3.330	VW
232	3.18	3.172	VW

[a] VS, very strong; S, strong; M, middle; W, weak; and VW, very weak.

during stretching and relaxation is quite typical in polyurethane.

3.2. Crystal structure of POSS molecules

The WAXD pattern from crystals of low-molar mass octacyclohexyl-POSS is depicted in Fig. 3. The complete list of the observed and calculated interplanar spacings is given in Table 1. The observed pattern can be fitted by a rhombohedral unit cell with parameters of $a = 11.57$ Å, $\alpha = 95.5°$. This structure is equivalent to a hexagonal unit cell with parameters of $a = 17.12$ and $c = 18.03$ Å. This result is consistent with a report by Barry et al. [25].

We also investigated the WAXD profiles of hydrido-POSS, which is depicted in Fig. 4. The observed and calculated interplanar spacings are listed in Table 2, which are almost identical to the data in Table 1. This result indicates that hydrido-POSS also has a rhombohedral unit cell with $a = 11.53$ Å, $\alpha = 95.3°$ or a correspondent hexagonal cell with $a = 17.06$ and $c = 18.01$ Å. This is an interesting observation because even though hydrido-POSS has a hydridomethylsiloxy corner group instead of the cyclohexyl group, it appears that the corner substitution has little effects on the crystal structure. One possible explanation is that the substituted group is freely rotating around the corner axis at room temperature, such that time-averaged WAXD profiles are almost identical between octacyclohexyl-POSS and hydrido-POSS. Further X-ray diffraction studies indicated
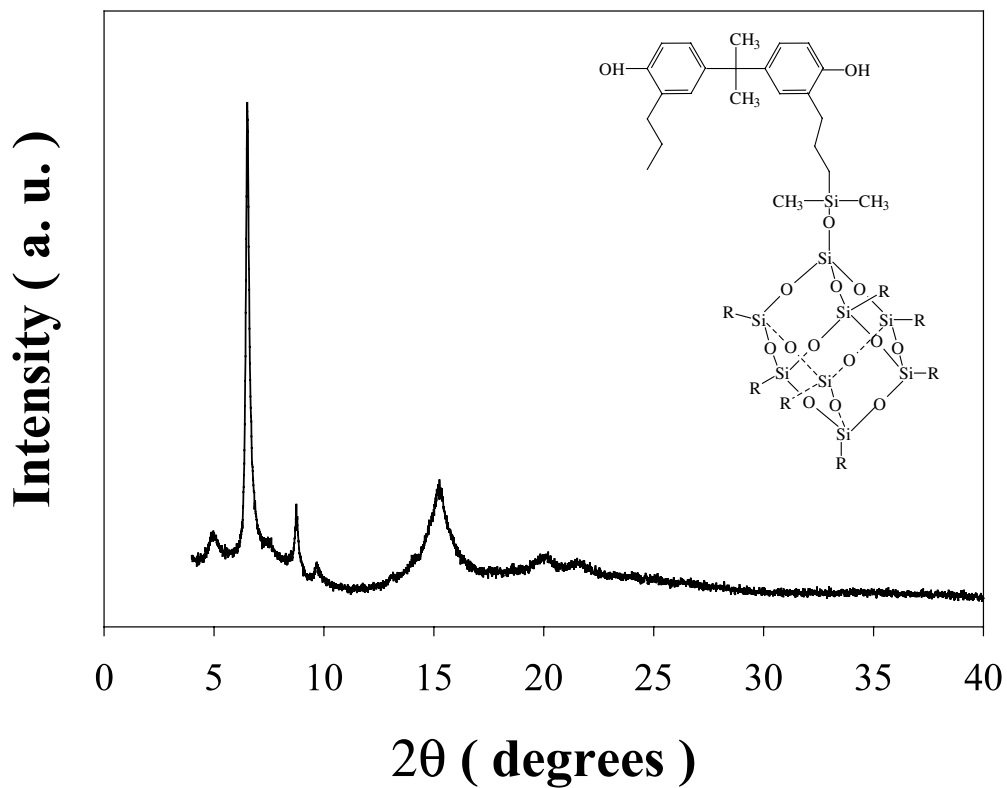
Fig. 5. The X-ray powder diffraction profile of BPA-POSS. This POSS monomer retains many major crystal reflections as those in hydrido-POSS.
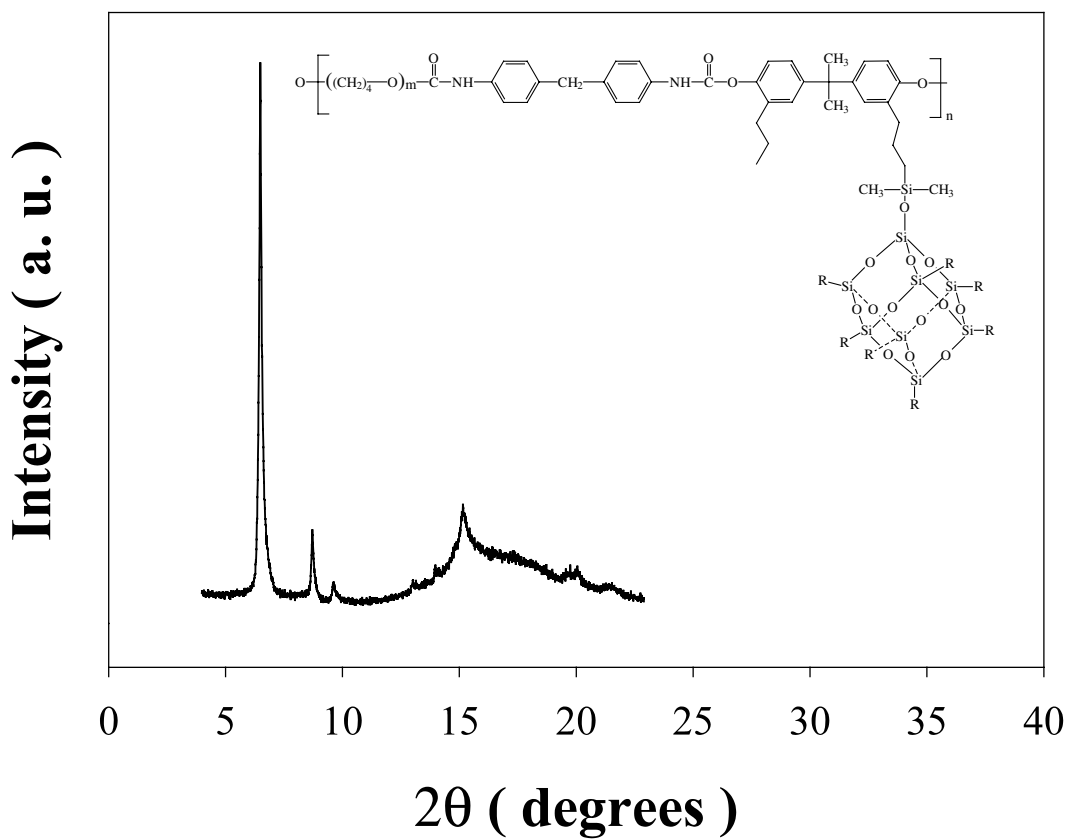

Fig. 6. The X-ray powder diffraction profile of POSS-PU-34. Some major crystal reflection peaks from the POSS monomer remain, which suggests that POSS molecules form nanoscale crystals in the hard segment domain.
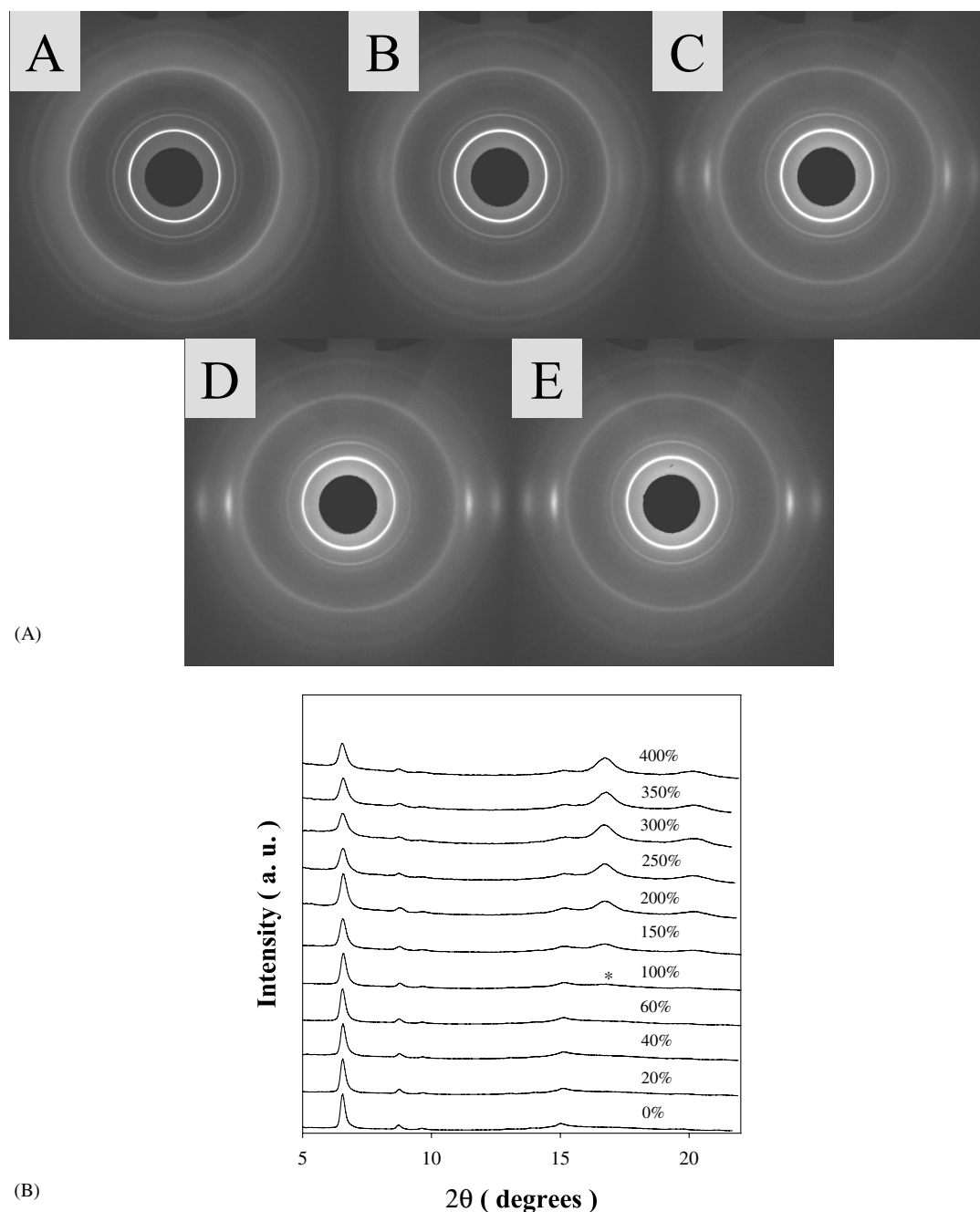
(A)

(B)

Fig. 7. (A) Two-dimensional WAXD patterns of POSS-PU-34 at stretching ratio of: (A) 0; (B) 100; (C) 200; (D) 300; and (E) 400%. The exposure time of each pattern was 1 min. (B) WAXD profiles of POSS-PU-34 along the equatorial direction at different strains. The symbol asterisk indicates the strain-induced crystallization of the soft segment.

that a phase transition indeed took place at low temperature (around −80°C), which will be published elsewhere. There are some differences between the diffraction profiles of octacyclohexyl-POSS and hydrido-POSS. First, all the crystal reflection peaks in hydrido-POSS are broader than that of octacyclohexyl-POSS, which indicates that the crystal size becomes smaller or more disordered by the substituted group. Second, some degrees of disordering are seen in the change of baseline. Finally, we notice that the 030 and 113 reflection peaks in octacyclohexyl-POSS can be clearly

separated, while in the hydrido-POSS, these two peaks are merged into one.

The WAXD profiles of the BPA-POSS monomer and POSS-PU polymer are shown in Figs. 5 and 6, respectively. Many reflection peaks are seen in the WAXD profile of BPA-POSS as those in hydrido-POSS. However, the introduction of the 3-(allylbisphenol-A) propyldimethylsiloxy group significantly increases the amorphous fraction. The first three peaks (101, 110, 012) still can be seen in the pattern but they are severely broadened. The peak shown
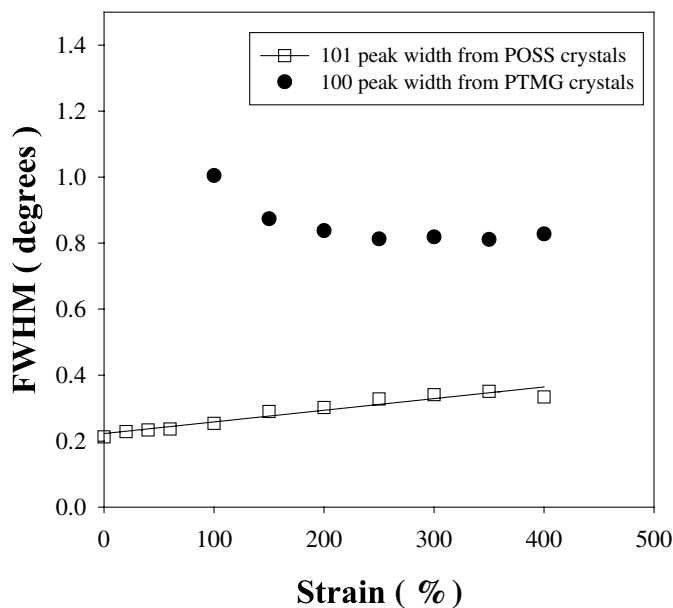
Fig. 8. The full width at half-maximum (FWHM) of the 101 peak of the POSS crystal and the 100 peak of soft segment (PTMG) crystals during stretching.

at 15.3° is the combination of 030, 113 and 122 reflections. The peak at 19.8° is the combination of 303 and 312 reflections. The last observable peak is at 21.5°, which is the combination of 124 and 105 reflections. When BPA-POSS is incorporated in the polyurethane (Fig. 6), the amorphous fraction becomes so large that some of the peaks are quite weak. However, the major peaks in the BPA-POSS can be clearly identified in polyurethane, which suggests that the grafted POSS molecules are probably aggregated and form nanoscale crystals.

3.3. In situ WAXD studies during deformation

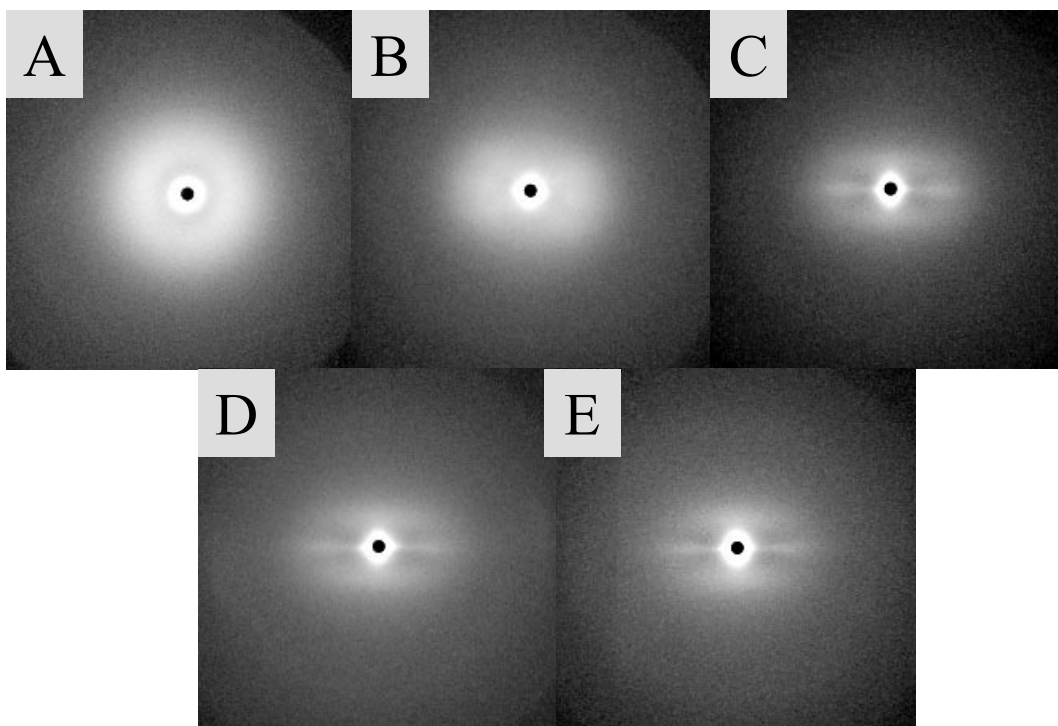WAXD data was collected during tensile deformation in

Fig. 9. Two-dimensional SAXS patterns of POSS-PU-34 at stretching ratio of: (A) 0; (B) 100; (C) 200; (D) 300; and (E) 400%. The exposure time of each pattern was 1 min.
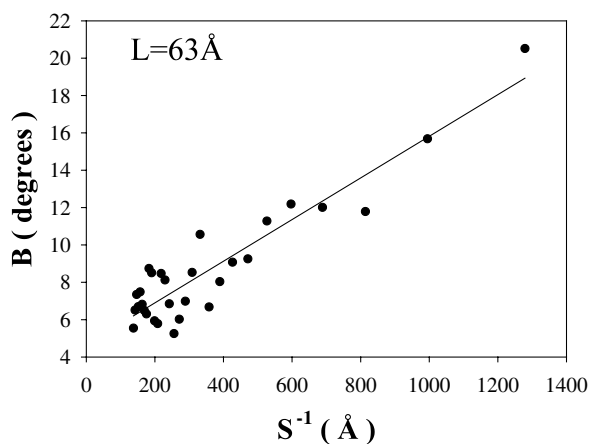
Fig. 10. Plots of B (the width of the angular intensity distribution of the azimuthal scan) versus s^{-1} for POSS-PU-34 at a strain of 400%. The crystal length calculated by the Ruland method is 63 Å.

order to determine the crystal structural changes in POSS and strain-induced crystallization of soft segment chains. Fig. 7A shows a series of WAXD patterns from the POSS-PU-34 sample recorded with imaging plates during deformation. The equatorial profiles extracted from the patterns are shown in Fig. 7B. Before stretching, the profile shows a broad amorphous polyurethane peak at about 15°, which is overlapped with 030, 113 and 122 reflection peaks from the POSS crystal. As the strain is above 100%, two reflection peaks resulted from the strain-induced crystallization of the soft segment (marked by an asterisk) are observed. These two peaks can be indexed as 100 and 101 reflections from the soft segment PTMG crystals. When the strain is above 200%, this strain-induced crystallization peak (PTMG crystals with good orientation) became dominant over the amorphous peak at 15°.

According to the Scherrer equation [26], the mean lateral dimension of the crystallites can be estimated from the breadth of the reflection peak (for e.g. the full width at half maximum, FWHM). The larger the FWHM, the smaller the crystal size. Fig. 8 shows the values of FWHM from the 101 peak of the POSS crystals and from the 100 peak of the soft segment PTMG crystals. The FWHM of the soft segment crystals before 100% cannot be reported because the peak does not exist. From this figure, it is seen that the FWHM of the soft segment 100 peak decreases with strain. The most significant decrease is observed between 100 and 200%. This observation indicates the behavior of strain-induced crystallization of the soft segments is enhanced. In contrast, the FWHM of the POSS crystals is found to increase almost linearly with strain. This suggests that partial POSS crystals were destroyed by deformation, probably through the annihilation of some hard segment domains, which has been verified by TEM and will be discussed later. At this point, we conclude that there is a reverse relationship between the formation of soft segment

crystals and the deformation of POSS crystals by mechanical deformation.

3.4. In situ SAXS studies during deformation

SAXS patterns were collected simultaneously during tensile deformation in order to monitor the changes in microphase domains. Typical SAXS patterns of the POSS-PU-34 sample stretched at different strains (to 400%) are shown in Fig. 9. In the initial state, the segmental microphase is clearly randomly oriented. The microphase separation between the hard and soft segment domains detectable by SAXS (having a spatial resolution less than 1000 Å) gives a ring in the pattern. In addition, a very strong diffuse scattering upturn is seen at low angles near the origin. This upturn may be due to the microphase having dimensions near or larger than the resolution limit of SAXS (~1000 Å). At 100% strain, the sample begins to show preferred orientation along the stretching direction, which results in an elliptical ring (long axis along the equator) in the pattern. When the strain becomes larger than 100%, the SAXS pattern showed a two-bar pattern with weak meridional peaks in the stretching direction and a stronger streak in the equatorial direction extended to large angles. The low-angle diffuse profile near the origin also shows a slight elongation in the stretching direction, which indicates that the average dimension of the larger second microphase is decreased by strain, a phenomenon also observed by TEM and will be discussed later. We attribute the meridional peaks to the oriented morphology of the microphase from the separation of hard and soft segments and the equatorial streak mainly to the extended crystal morphology of the strain-induced soft segment crystals. We come to this conclusion based on several observations. (1) The long period of the initial unoriented sample is about the same as the long period in the meridian of the oriented sample, which indicates that deformation realigns part of the microphase (detectable by SAXS) along the stretching direction. (2) The intensity of the equatorial streak, although stronger than the meridional peak, is substantially weaker than that of the central diffuse scattering. Judging by the low level of the equatorial intensity, we rule out the possibility of void scattering. (3) The corresponding WAXD profiles (Fig. 7A) indicate that the strain-induced crystallization in the soft segments completely coincides with the occurrence of the equatorial streak. Although there are other possibilities that may also contribute to the equatorial streak such as the deformed hard segment domains or the aligned POSS nanocrystals, we believe these contributions are relatively small.

At high strains, the equatorial scattering streak (assumed mainly due to the strain-induced soft segment crystals) can be analyzed by Ruland's method [27,28] to estimate the microfibrillar structure as follows:

$$B_{obs} = 1/(Ls) + B_\phi \qquad (1)$$

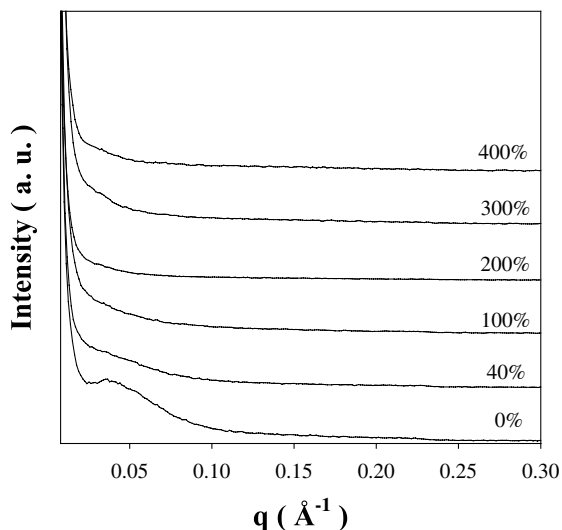where B_{obs} is the integral breadth of the intensity profile

Fig. 11. SAXS profiles of POSS-PU-34 along the meridional direction at different strains.

obtained along the azimuthal scan and B_ϕ is the integral breadth due to misorientation of the scattering objects, s is the scattering vector defined as $2(\sin\theta)\lambda^{-1}$ (2θ being the scattering angle) and L is the length of the microfibrillar structure. The term ($1/LS$) represents the integral breath due to length distribution of the scattering objects. Eq. (1) assumes that all the scattering profiles (azimuthal) have a Lorentzian function form. The underlying physics of this approach is that both size distribution and orientation distribution of the scatterers can contribute to the broadening of the scattering profile. By using the integral breadth (along the azimuthal scan) method, these two effects (size and misorientation) can be separated. The average soft segment crystal length can be estimated by plotting B_{obs} vs. s^{-1}, as shown in Fig. 10. Using this method, the average length of the microfibrillar soft segment crystal structure at 400% deformation strain is about 60 Å. This value may be underestimated if there is another scattering object with different size and orientation also contributing to the equatorial streak.

The scattering intensity $I(q)$ measured from the partially oriented three-dimensional object can be transformed to the one-dimensional intensity $I_1(q)$ by Lorentz correction,

$$I_1(q) = cI(q)q^2 \tag{2}$$

where c is a constant and $q = 2\pi s$. In this case, the meridional sliced SAXS data can be analyzed via the correlation function $\gamma(r)$,

$$\gamma(r) = \int_0^\infty I_1(q)\cos(qr)\,\mathrm{d}q/Q \tag{3}$$

where Q is the invariant defined as $Q = \int_0^\infty I_1(q)\,\mathrm{d}q$. With the correlation function method [29], the average long period between the hard segment domains of POSS-PU-34 can be estimated to be 110 Å and POSS-PU-0 [30] to be 190 Å. The smaller long period in POSS-PU-34 indicates a denser distribution of the hard segment domains (at least in the view of SAXS), which may be attributed to a superior mechanical property. Fig. 11 shows the SAXS profiles of POSS-PU-34 along the meridional stretching direction during deformation. At the undeformed state, POSS-PU-34 shows a peak in the Lorentz corrected profile around 0.06 Å^{-1} (in q, or around 0.04 Å^{-1} in the as measured profile in Fig. 11) which can be interpreted as a typical microphase separation structure in segmented polyurethane. At all applied strains, this peak appears to be at a constant position, even though it becomes weaker. The decrease in the scattering intensity (normalized by sample absorption) suggests a decrease of the hard segment domain fraction. However, the constant peak position indicates that the remaining microphase morphology of the hard and soft segments, in the range detectable by SAXS, persists at high deformation strains and even under the presence of strain induced crystallization in soft segments. One possibility is that the hard segment domains having chains normal to the strain direction may be destroyed or realigned, whereas the domains with chains along to the stretching direction may stay intact. The destruction or deformation of the domains through chain pulling out seems to be inevitable. Another interesting observation is that if some domains become elongated, the average long spacing between the adjacent domains remains unchanged.

3.5. TEM characterization

Fig. 12 shows the TEM micrographs of unstretched (Fig. 12A) and stretched (Fig. 12B and C) POSS-PU-34. In TEM-imaging of the POSS segmented urethanes, the hard segment domains appear as a dark phase due to the high electron density afforded by POSS molecules, relative to the hydrocarbon soft segment phase. The formation of nanoscale POSS crystals thus resides within or adjacent to the hard segment domains. The relative large fraction of the dark phase (hard segment domains) is due to the projection of all hard segment domains in a sample of 700 Å thickness. It can be seen in Fig. 12A that POSS domains within unstretched POSS-PU-34 show irregular shape and size, making it difficult to precisely determine their sizes. Nevertheless, characteristic lengths span 50–2500 Å. Previously, we have performed the TEM on thin film cast from dilute solution of POSS-PU-34, which showed spherical hard segment domains with a broad size distribution [31]. We suggest that, in this study, domains are initially spherical; they deform and coalesce into irregular shapes (most of them disk-like) and varying sizes during the compression molding. As can be seen in Fig. 12A, the coexistence of relatively small ellipsoidal and large spherical domains can be observed, and several hard segment domains aggregate to form big domains (see lower left corner in Fig. 12A). The average spacing between the small domains is in the order of 100 Å, which is consistent with the long spacing determined by SAXS. The existence of the large microphase
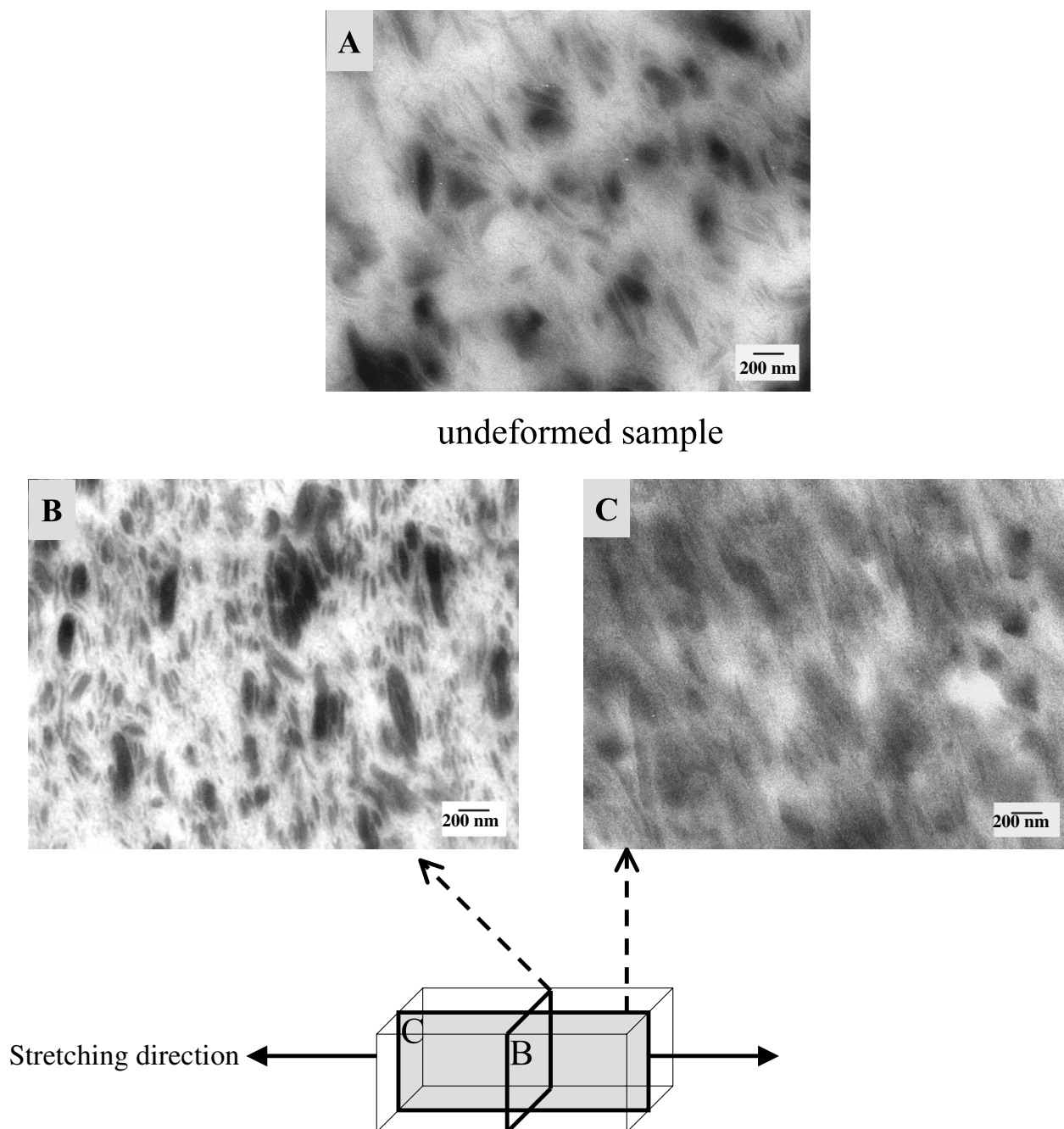
Fig. 12. Transmission electron microscopy (TEM) images of POSS-PU-34 which was cryo-microtomed to film thickness approximately 700 Å in thickness: (A) undeformed sample; (B) drawn sample cryo-microtomed with the normal along the stretch direction; and (C) drawn sample cryo-microtomed with the normal perpendicular to the stretch direction.

domains (>1000 Å) is consistent with the observation of the low-angle SAXS upturn. Two factors may contribute to the existence of different shapes of hard segment domains. First, the cutting (by microtoming) of disk-shaped domains in different orientations naturally yields a distribution of shapes and sizes. Second, it is conceivable that the larger hard segment domains feature a higher concentration of POSS aggregates such that deformation and break-up by compression molding and microtoming are resisted by enhanced mechanical properties.

In contrast to unstretched film, Fig. 12B shows the TEM image of a section whose normal follows the stretching direction. In this case, the area fraction (concentration) of hard domains is apparently higher than in the unstretched state, indicating a tendency for lateral compression during the stretching process to nucleate and cause aggregation of hard segment domains. In addition, hard segment domains show larger and more regular ellipsoidal shape compared to the unstretched film. Inspection of the orthogonal view (i.e. along the stretch direction) is shown in Fig. 12C, where the
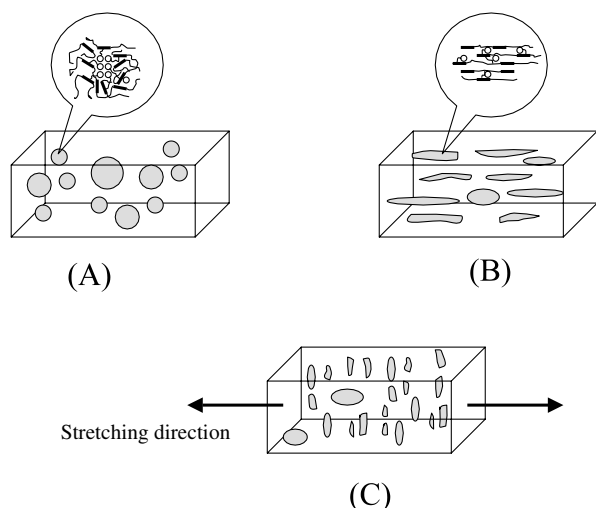
Fig. 13. Schematic diagram of microphase changes during stretching. (Rings indicate the POSS molecules, bars represent the hard segments. The stretching direction is horizontal. Some large hard segment domains are purposely-missed here.): (A) no deformation or low deformation (POSS molecules form nanocrystals in the hard segment domains); (B) intermediate deformation (e.g. 400%) (some POSS crystals are destroyed in the hard segment domains); and (C) large deformation after relaxation (e.g. 700%) as in TEM.

stretching direction is horizontal. Surprisingly, most of hard segment domains are preferentially aligned along a direction perpendicular to the stretching direction. Additionally, the aspect ratio of domains imaged in this view is much larger than in the view along the stretching direction, to an extent that the domain thickness is difficult to resolve. The hard-segment domains imaged in Fig. 12B, from a cut parallel to the plane of disks, appear relatively large. In contrast, the size of hard segment domains is reduced in Fig. 12C because of cutting along the disk normal. Thus, tensile stretching of POSS-PU-34 leads to deformation of hard segment domains into disk-like domains with plane normals almost parallel to the stretching direction.

A schematic diagram of microphase changes (domains larger than 1000 Å are ignored here) in POSS-PU during stretching is shown in Fig. 13, based on results from TEM and X-ray studies. Fig. 13A indicates the original state of the hard segment domain distribution. The hard segment domains (dark regions) are randomly dispersed in the soft segment matrix and with a large distribution of size. The POSS crystals possibly reside inside these domains. After stretching to a higher ratio (e.g. 400%, Fig. 13B), hard segment domains can be elongated as well as the soft segments. Some of the POSS crystals are destroyed under the stress due to the pullout of the chains in the hard segment domains. At further stretching, some large hard segments are broken into small disk-like pieces with plane normals almost parallel to the stretching direction, which can be observed by TEM of the relaxed sample.

4. Conclusion

We have studied the structural development of a unique polyurethane system having inorganic POSS molecules attached to the hard segments as nanoscale reinforcing agents. The tensile test showed that the incorporation of POSS molecules greatly enhanced the tensile modulus and the strength. The X-ray powder diffraction method was used to determine the crystal structure of two kinds of POSS monomers. One was octacyclohexyl-POSS, which showed a rhombohedral unit cell with $a = 11.57$ Å, $\alpha = 95.5°$. The other was hydrido-POSS, which showed a similar rhombohedral unit cell with $a = 11.53$ Å, $\alpha = 95.3°$. A systematic X-ray pattern change was observed from POSS monomers to POSS-PU polymer, with increase in amorphous fraction and large disordering in the structure. Simultaneous WAXD and SAXS techniques were applied to reveal the POSS crystal structural and POSS-PU morphological changes under deformation. The WAXD data indicated that POSS molecules formed nanoscale crystals in the hard segment domains. Under stretching, the full width at half-maximum of the POSS crystal peak was found to decrease, which suggested the destruction of POSS crystals and also the hard segments. The SAXS data showed that at strains larger than 100%, the microphase structure of POSS-PU was oriented along the stretching direction. The decrease in the scattering intensity indicates that hard segment domains were partially destroyed, which was consistent with the WAXD observation. At strains above 200%, the SAXS pattern showed an intense streak along the equatorial direction, which was attributed to the microfibrillar structure of the strain-induced crystallization of the soft segments, which is also evident by WAXD. The average length of the extended PTMG crystal at high strains was about 60 Å estimated by the Ruland method. TEM observations on a stretched and relaxed POSS-PU-34 sample indicated that tensile stretching broke the large hard segment domains into disk-like domains with plane normals almost parallel to the stretching direction.

References

[1] Bonart R. J Macromol Sci -Phys B 1968;2(1):115.

[2] Koberstein JT, Leung LM. Macromolecules 1992;25:6205.

[3] Koberstein JT, Galambos AF, Leung LM. Macromolecules 1992;25:6195.

[4] Bonart R, Morbitzer L, Hentze G. J Macromol Sci -Phys B 1969;3:337.

[5] Bonart R, Morbitzer L, Müller EH. J Macromol Sci -Phys B 1974;9:447.

[6] Bonart R, Müller EH. J Macromol Sci -Phys B 1974;10:117.

[7] Koberstein JT, Stein RS. J Macromol Sci -Phys Ed 1983;21:1439.

[8] Koberstein JT, Leung LM. J Macromol Sci -Phys Ed 1985;23:1883.

[9] Lichtenhan JD, Noel CJ, Bolf AG, Ruth PN. Mat Res Soc Symp Proc 1996;435:3.

[10] Haddad TS, Lichtenhan JD. Macromolecules 1996;29:7302.

[11] Mather PT, Romo-Uribe A, Otonari Y, Carr MJ, Lichtenhan JD. Soc Plast Eng Symp Proc 1997:1817.

[12] Haddad TS, Farris AR, Lichtenhan JD. Am Chem Soc Polym Prep 1997;38(1):127.

[13] Mather PT, Chaffee KP, Haddad TS, Lichtenhan JD. Am Chem Soc Polym Prep 1996;37(1):765.

[14] Mather PT, Jeon HG, Romo-Uribe A, Haddad, TS, Lichtenhan JD. Macromolecules 1998;32:1194.

[15] Voronkov MG, Lavrent'yev VI. Top Curr Chem 1982;102:199.

[16] Baney RH, Itoh M, Sakakibara, A, Suzuki T. Chem Rev 1995;95:1409.

[17] Lichtenhan JD. Comments Inorg Chem 1995;17:115.

[18] Lichtenhan JD, Vu NQ, Carter JA, Gilman JW, Feher FJ. Macromolecules 1993;26:2141.

[19] Haddad TS, Lichtenhan JD. J Inorg Organomet Polym 1995;5:237.

[20] Gilman JW, Schlitzer DS, Lichtenhan JD. J Appl Polym Sci 1996;60:591.

[21] Scott DW. J Am Chem Soc 1946;68:356.

[22] Schwab JJ, Lichtenhan JD, Carr MJ, Chaffee KP, Mather PT, Romo-Uribe A. Am Chem Soc Polym Prep 1997;77:549.

[23] Cella RJ. J Polym Sci, Part C 1973;42:727.

[24] Witsiepe WK. Adv Chem Ser 1973;129:39.

[25] Barry J, Daudt WH, Domicone JJ, Gilkey JW. J Am Chem Soc 1955;77:4248.

[26] Scherrer P. Gõttinger Nachrichten 1918;2:98.

[27] Ruland W. J Appl Crystallogr 1970;3:525.

[28] Ruland W. J Polym Sci, Part C 1969;28:143.

[29] Hsiao BS, Verma RK. J Synchrotron Rad 1998;5:23.

[30] Fu B, Hsiao B, White H, Rafailovich M, Mather P, Jeon H, Phillips S, Lichtenhan J, Schwab J. Polym Int 2000;49:437.

[31] White H, Rafailovich M. Unpublished TEM results.